Single Ions Trapped in a One-Dimensional Optical Lattice

Martin Enderlein,[1,2] Thomas Huber,[1,2] Christian Schneider,[1,2] and Tobias Schaetz[1,2,*]

[1]*Physikalisches Institut, Albert-Ludwigs-Universität Freiburg, Hermann-Herder-Strasse 3, 79104 Freiburg, Germany*
[2]*Max-Planck-Institut für Quantenoptik, Hans-Kopfermann-Strasse 1, 85748 Garching, Germany*

We report on three-dimensional optical trapping of single ions in a one-dimensional optical lattice formed by two counterpropagating laser beams. We characterize the trapping parameters of the standing-wave using the ion as a sensor stored in a hybrid trap consisting of a radio-frequency (rf), a dc, and the optical potential. When loading ions directly from the rf into the standing-wave trap, we observe a dominant heating rate. Monte Carlo simulations confirm rf-induced parametric excitations within the deep optical lattice as the main source. We demonstrate a way around this effect by an alternative transfer protocol which involves an intermediate step of optical confinement in a single-beam trap avoiding the temporal overlap of the standing-wave and the rf field. Implications arise for hybrid (rf-optical) and pure optical traps as platforms for ultracold chemistry experiments exploring atom-ion collisions or quantum simulation experiments with ions, or combinations of ions and atoms.

Offering unique operational fidelities and individual addressability, atomic ions in radio-frequency (rf) traps are one of the most successful and promising systems for quantum computation [1,2] and quantum metrology [3]. Because of strong short- as well as long-range interactions in Coulomb crystals, they are also predestined for quantum simulation experiments [4] of, e.g., solid-state physics models [5–7]. However, experiments on the quantum level with ions in rf traps have been limited to the order of ten ions arranged in a linear string and a common trapping potential [8,9]. Experimental approaches to scaling particle numbers and dimensionality of trapped-ion quantum simulations are mainly based on surface-electrode microtrap arrays [7,10–12] and Penning traps [13].

Extending the recent demonstration of ion trapping in a single-beam dipole trap [14,15] to optical lattices has been proposed [16] to offer an alternative route to scaling by combining the advantages of Coulomb interactions with the scalability and versatility that have been developed for optical lattices [17]. Such a system additionally allows for storing ions and atoms in a common trap. This may become essential [18] for ultracold atom-ion collision experiments [19–22] because of the strong suppression of micromotion [23]. In this context optical lattices may be useful, be it to increase trap depths, store several ions or atoms in separate microwells, or as conveyor belts [24] for individual ions and atoms.

In the past, standing-waves were already used in combination with ions and rf traps to study particle dynamics [25] and were considered for preparing nonclassical motional states [26] as well as implementing forces that depend on the electronic state [5,16]. Additionally, there are proposals for quantum simulations requiring the local shaping of the trapping potential of a rf-trapped Coulomb crystal by an optical lattice [27,28].

Here we report on trapping single ions in an all-optical trap, where the confinement along the laser beam direction is provided by an optical lattice, while the rf trap is switched off.

Figure 1 shows a schematic of our setup. The experiments start by initializing single ^{24}Mg$^+$ ions (nuclear spin $I = 0$) in a linear rf trap ($\omega_{\rm rf} = 2\pi \times 56$ MHz) [29]. This includes the creation of an ion by photoionization from a
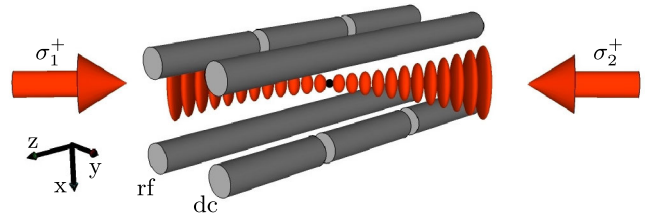

FIG. 1 (color online). Schematic of the setup. The linear rf trap consists of four electrode rods. The rf voltage is applied to two rods while the others (segmented) remain at rf ground. This generates a two-dimensional confinement in the radial (x/y) directions. Additional dc voltages applied to the outer electrode segments add the axial confinement (z direction). The counter-propagating dipole trap beams (arrows) propagate in the y-z plane, crossing the z axis at an angle of 45°. They are focussed on the ion at the center of the rf and dc potentials (black dot) and have waist radii of $w_0 \approx 5$ μm, and equal intensities. The non-interfering configuration $\{\sigma_1^+, \sigma_2^-\}$ leads to a Gaussian-shaped dipole potential (not shown) with twice the single-beam intensity. For identical polarizations $\{\sigma_1^+, \sigma_2^+\}$, the two beams interfere and form an additional standing-wave pattern in the direction of beam propagation, as shown. At the positions of constructive interference, the maximal intensity ideally is 4 times that of the single beam. Not shown are additional Doppler cooling beams (propagating in the x-z plane at an angle of 22.5° to the z axis). Doppler cooling fluorescence light from the ion is detected with a CCD camera above the trap.

thermal atomic beam and Doppler cooling to a few mK (Doppler cooling limit: 1 mK). Initially, the oscillation frequencies of the ions in the ponderomotive, i.e., time-averaged, potential of the rf trap are $\omega_{x,y} \approx 2\pi \times 860$ kHz radially and $\omega_z \approx 2\pi \times 110$ kHz axially.

Two dipole trap beams are arranged in a counterpropagating configuration, providing light at a wavelength of $\lambda = 280$ nm and a power $P_{dip} \leq 100$ mW in each beam [30]. The dipole trap beams are red detuned ($\Delta_{dip} \approx -2\pi \times 290$ GHz) from the $S_{1/2}$-$P_{3/2}$ transition. The polarization of the beams can either be tuned to $\{\sigma_1^+, \sigma_2^-\}$, denoting the noninterfering configuration where beam #1 has σ^+ and beam #2 σ^- polarization, or both beams are σ^+ polarized, $\{\sigma_1^+, \sigma_2^+\}$, which allows for their interference. Coupling the $S_{1/2}$ states to the $P_{3/2}$ multiplet by the different polarization configurations relates to different light shifts and, thus, dipole potentials of different depths for identical laser intensities. To permit a direct comparison between the two configurations we consider the saturation parameter

$$s_{dip} = c \frac{I_{dip}/I_{sat}}{1 + (2\Delta_{dip}/\Gamma)^2} \leq 3 \times 10^{-3},$$

with a linewidth $\Gamma = 2\pi \times 41.8$ MHz, a saturation intensity $I_{sat} = 250$ mW/cm^2, and the single-beam intensity I_{dip}. The coupling strength is $c = 1$ for $\{\sigma_1^+, \sigma_2^+\}$ and $c = \frac{2}{3}$ for $\{\sigma_1^+, \sigma_2^-\}$.

In the first stage of the experiment we compare the light shifts induced by a single Gaussian laser beam $\{\sigma_1^+\}$ with that of two counterpropagating beams $\{\sigma_1^+, \sigma_2^+\}$ in order to calibrate the interference of the dipole trap beams and to obtain estimates on the relevant experimental imperfections. We trap an ion in the rf trap and simultaneously induce a light shift. We then detect the fluorescence of the ion induced by an additional low-power probe beam as a function of s_{dip} of the dipole trap beam(s). The probe beam is σ^+ polarized and has an on-resonance saturation parameter $s_0 \approx 0.3$. It is overlapped with one of the dipole trap beams and is (blue) detuned by $\Delta_{probe} = 2\pi \times 455$ MHz $\approx 10\Gamma$ with respect to the unshifted $S_{1/2}$-$P_{3/2}$ transition. Thus, resonance with the probe laser occurs when the light shift induced by the dipole trap beam(s) matches the detuning of the probe laser. With all lasers σ^+ polarized, we drive the closed cycling transition $|^2S_{1/2}, m_J = \frac{1}{2}\rangle \leftrightarrow |^2P_{3/2}, m_J = \frac{3}{2}\rangle$ and the relevant energy levels reduce to a two-level system.

The results are shown in Fig. 2. For zero s_{dip}, the probe laser is far detuned, causing a negligible fluorescence rate. Increasing the power of the dipole trap beam(s) and, thus, s_{dip}, provides an increasing light shift. The electronic transition approaches resonance with the probe laser, resulting in an increasing fluorescence rate. The measurement with a single dipole trap beam serves as a reference. Its maximal fluorescence rate occurs at $s_{dip} \approx 1.28 \times 10^{-3}$. In the measurement with $\{\sigma_1^+, \sigma_2^+\}$ we find the resonance at lower s_{dip} since less single-beam power is needed to shift
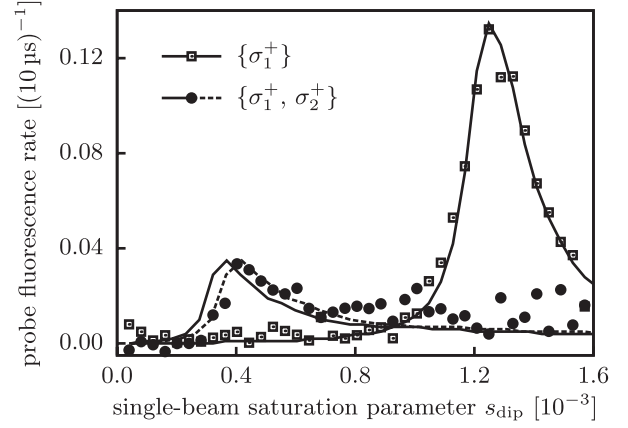

FIG. 2. Measurement of the light shift induced by the dipole trap beam(s) on an ion stored in the rf trap. The fluorescence of an ion due to a weak, blue-detuned probe laser is measured as a function of the single-beam saturation parameter s_{dip} of the dipole trap beam(s). The two configurations of the dipole trap beams are either a single Gaussian beam $\{\sigma_1^+\}$ or a combination of two counterpropagating beams $\{\sigma_1^+, \sigma_2^+\}$. The detection time is 10 μs. Each data point is the average of 4000 measurements. Statistical errors of the fluorescence measurements are small compared to the size of the symbols. Statistical errors due to the subtraction of stray light, measured without ion, lead to an increasing variance for increasing s_{dip} and are not considered in the error budget. The systematic error of s_{dip} corresponds to an uncertainty of the absolute values of the s_{dip} scale, which is not relevant here. Solid lines show the results of MCSs with $T_0 = 3.5$ mK. The dashed line is a fit of the MCS to the measured resonance in the counterpropagating configuration. From this we derive an estimate for experimental imperfections requiring the higher s_{dip} to shift the transition into resonance with the probe laser.

the transition into resonance with the probe laser. The resonance is reduced in amplitude by a factor of 3 and broadened towards higher s_{dip}.

We compare the experimental results with Monte Carlo simulations (MCS) treating laser-ion interaction in rate equations [15] and relying on the ponderomotive approximation for the rf trap potential. With the assumption of a thermal initialization of the ions at $T_0 = 3.5$ mK [31], the simulation is in good agreement with the measurement results. This confirms the formation of a standing-wave at the position of the ion. The shapes and amplitudes of the resonances can be explained by the oscillations of the ion in the combined trap consisting of the rf and the optical potential. In particular, the broadened resonance in the standing-wave case as well as the shift of the fluorescence maximum to $s_{dip} \approx 0.37 \times 10^{-3}$ in the MCS, compared to its ideal location at a quarter of the single-beam resonance, $s_{dip} \approx 1/4 \times 1.28 \times 10^{-3} = 0.32 \times 10^{-3}$, are due to the spatially averaged, and therefore reduced, light shift which the oscillating ion experiences. The experimental resonance in the standing-wave case occurs at $s_{dip} \approx 0.42 \times 10^{-3}$. This additional shift of the saturation parameter scale by $\approx 12\%$ (see dashed line in Fig. 2) hints

at an imperfect overlap of the dipole trap beams due to, e.g., beam-pointing instabilities, corresponding to an average displacement of the two beams by $\approx 1~\mu$m. We use this result as an input for the MCSs of the optical trapping experiments discussed in the following.

In the next stage of the experiment, we switch off the rf confinement completely and measure the trapping probability for a constant trapping time as a function of $s_{\rm dip}$ in optical traps formed by counterpropagating dipole trap beams, either interfering, $\{\sigma_1^+, \sigma_2^+\}$, or noninterfering, $\{\sigma_1^+, \sigma_2^-\}$. Considering the chosen parameters and related heating rates, the result for the trapping probability in the standing-wave trap (optical lattice) can outperform that in the noninterfering dipole trap for small $s_{\rm dip}$ and short trapping times only. In this regime, the effect of the additional trap depth due to the interference still overcomes the increased dipole-force fluctuation heating in the standing-wave [33].

The experimental sequence is the following: in order to optimize the transfer between rf trap and optical trap, we first carefully compensate stray electric fields (for a quantitative estimate, see below). This is done by ramping down the rf potential to $\omega_{x,y} \approx 2\pi \times 100$ kHz and counteracting the displacement of the ion with appropriate dc voltages [15]. For the optical trapping attempts, we ramp up the two counterpropagating dipole trap beams and, subsequently, ramp the rf potential down to zero, each in 50 μs. After the optical trapping time $T_{\rm opt}$, the transfer protocol is reversed and the ion is detected via resonance fluorescence in case of successful optical trapping. During all steps a static electric potential in the z direction ($\omega_z = 2\pi \times 45$ kHz) is retained, such that, in the noninterfering case, the total confinement is due to the dipole plus the static electric potential. Compared to the standing-wave confinement, the contribution of the static electric potential remains negligible. According to Laplace's equation, its focusing effect along the z axis even comes at the price of a defocusing effect in at least one radial direction, which has to be overcome by the optical potentials [15].

Figure 3 shows the trapping results for $T_{\rm opt} = 25~\mu$s. For both polarization configurations, at $s_{\rm dip} = 0$, and thus zero optical trap depth, the trapping probability is found to be zero, verifying that after turning off the rf trap there remain no significant residual trapping potentials [34]. In the noninterfering case the optical trapping probability rises with increasing $s_{\rm dip}$ and reaches close to $P = 100\%$. In the standing-wave case, the trapping probability exceeds that of the noninterfering case for $s_{\rm dip} \lesssim 0.6 \times 10^{-3}$, but then levels off at $P \approx 80\%$.

The gradual rise of optical trapping probability with increasing $s_{\rm dip}$ is due to the nonzero initial temperature. For the standing-wave case, the trapping probability rises faster due to the trap depth being increased, ideally, by a factor of 2. The reduced trapping probability for $s_{\rm dip} > 1 \times 10^{-3}$ cannot be explained by laser-induced heating effects because these should remain negligible within this regime [33] (the explanation follows in the context of Fig. 4).
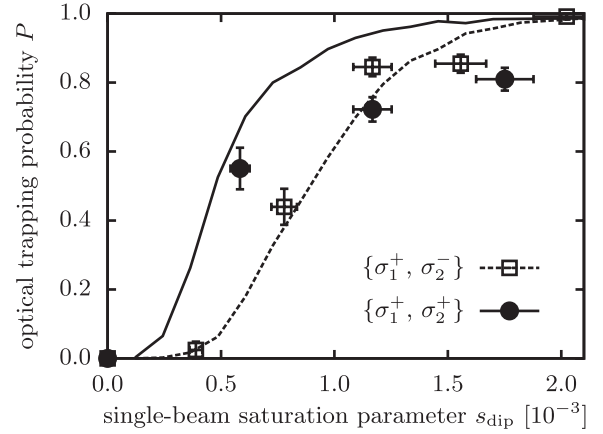

FIG. 3.   Optical trapping probability as a function of the single-beam saturation parameter for the noninterfering, $\{\sigma_1^+, \sigma_2^-\}$, and the interfering, $\{\sigma_1^+, \sigma_2^+\}$, configuration of the two counterpropagating dipole trap beams. The optical trapping time is $T_{\rm opt} = 25~\mu$s. Data points represent the mean number of successful trapping attempts for typically 30 ions with 1σ statistical errors for the trapping probability and systematic errors for the saturation intensity ($\delta P_{\rm dip}/P_{\rm dip} = \pm 0.03$, $\sigma_{w_0} \approx 0.27~\mu$m). Lines represent MCS results based on the ponderomotive approximation to the rf potential. Input parameters are $T_0 = 3.5$ mK, a power scaling factor of 0.88, and an offset force $F = 0.9 \times 10^{-20}$ N (see also Ref. [31]).

Shown in Fig. 3 are also the results of the MCSs. These incorporate the full transfer sequence of the ion from the ponderomotive potential of the rf trap into the dipole trap (as in Ref. [15]) as well as dressed-state rate equations [35], which allow us to reproduce both recoil heating and dipole-force fluctuation heating [33].

In the noninterfering case, good agreement with the measurements is obtained, again assuming $T_0 = 3.5$ mK. The small trapping probability at $s_{\rm dip} \approx 0.4 \times 10^{-3}$ is reproduced assuming a constant force $F = 0.9 \times 10^{-20}$ N radial to the trapping beam. This gives an estimate for the limitation of our stray-field compensation procedure and matches very well the rough calculation of $F = 10^{-20}$ N which we made in Ref. [14]. The simulation in the standing-wave case, again with $T_0 = 3.5$ mK, reproduces the faster rise at small $s_{\rm dip}$. However, it also predicts $P \approx 100\%$ for $s_{\rm dip} > 1.5 \times 10^{-3}$, which is not observed in the experiment.

Remarkably the harmonically approximated oscillation frequency along the standing-wave direction reaches $\omega_{\rm dip} \approx 2\pi \times 30$ MHz $\approx \omega_{\rm rf}/2$ at $s_{\rm dip} \approx 3 \times 10^{-3}$. To reveal the causal link between the reduced trapping probabilities and the rf field, we modify the previous (direct transfer) protocol of loading the ion from the rf trap into the standing-wave trap: we insert the transfer into a single-beam optical trap and ramp up the second dipole trap beam only after the rf amplitude has been ramped down to zero (indirect transfer). Thus, we avoid the temporal overlap of standing-wave and rf field.
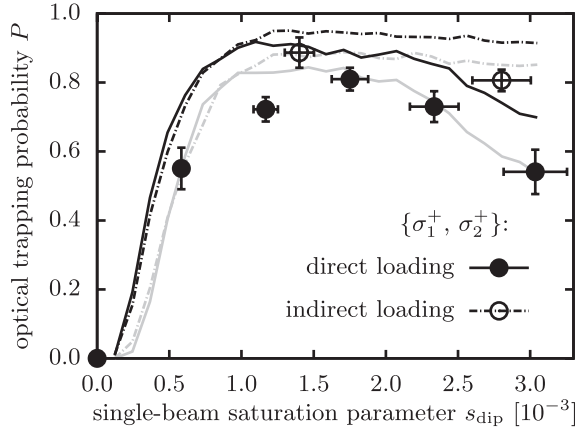
FIG. 4.   Optical trapping probability as a function of the single-beam saturation parameter for the interfering configuration, $\{\sigma_1^+, \sigma_2^+\}$. Comparison of two different protocols for loading of the optical lattice: direct transfer from the rf trap to the optical lattice (as in Fig. 3, $T_{\rm opt} = 25\ \mu$s) and indirect loading via an intermediate phase of trapping in a single-beam trap ($T_{\rm opt} = 100\ \mu$s). Data points represent the mean number of successful trapping attempts for typically 30 ions with 1σ statistical errors for the trapping probability and systematic errors for the saturation intensity (see Fig. 3). Lines show MCS results for both loading sequences, taking into account the time-dependent rf potential (input parameters as in Fig. 3). Gray lines represent MCS results that consider additional experimental imperfections.

The results for single-beam saturation parameters of $s_{\rm dip} \approx 1.5 \times 10^{-3}$ and $s_{\rm dip} \approx 2.8 \times 10^{-3}$ are shown in Fig. 4. Also depicted are the experimental results for the direct transfer process from Fig. 3 with the extended range of $s_{\rm dip} \leq 3 \times 10^{-3}$, where for $s_{\rm dip} > 1.5 \times 10^{-3}$ the increase of $s_{\rm dip}$ leads to a decrease of the trapping probability to below 60%. In contrast with the indirect transfer, we significantly increase the trapping probability, e.g., by 30% at $s_{\rm dip} = 2.8 \times 10^{-3}$.

Still, these results represent a lower bound to the actual improvement since additional losses occur during the single-beam trapping phase with $s_{\rm dip} \approx 2.8 \times 10^{-3}$ and the increase of the optical trapping time to $T_{\rm opt} = 100\ \mu$s, as required for the extended protocol.

Figure 4 also shows results of MCSs that incorporate the time-dependent rf potential. For the direct transfer, the drop in trapping probability for $1.5 \times 10^{-3} < s_{\rm dip} < 3 \times 10^{-3}$ is reproduced well. For the indirect transfer we retrieve the significantly increased trapping probabilities. This is evidence that the observed reduction in trapping probability for the direct transfer is mainly due to excitation of the ion motion within the stiff potential of the standing-wave by the rf driving field: $\omega_{\rm dip}$ approaching $\omega_{\rm rf}/2$ leads to increasing parametric excitations. This may also explain results we obtained with hybrid traps consisting of the rf potential and red- or blue-detuned standing-waves, where the optical trapping probability deteriorated compared to the exclusively optical confinement described above. For both transfer

protocols of Fig. 4, the observed trapping probabilities remain below the simulation results. This, presumably, is a result of additional experimental imperfections. For the direct loading, for example, spatially not perfectly overlapped traps (offset $\vec{d}$) lead to additional micromotion during transfer, which amplifies the parametric excitation. In fact, by adapting the MCS parameters to $F = 1.7 \times 10^{-20}$ N and $\vec{d} = 0.35\ \mu$m $\times \vec{e}_x$, very good agreement between simulation and experiment can be reached (gray lines in Fig. 4).

Our results might have to be considered in future experiments, in particular for hybrid (rf-optical) traps such as those currently used [20–22] and proposed [18] for ultracold atom-ion collision experiments or quantum simulations [27,28]. Apart from the method of indirect loading, demonstrated here, possible ways to minimize rf heating of the ion are high radio frequencies, far beyond the oscillation frequencies in the lattice, and/or low oscillation frequencies in the lattice due to longer wavelengths. A standing-wave aligned with the rf trap axis could reduce rf-induced parametric heating by minimizing the projection of rf forces on the standing-wave direction. If a blue-detuned laser was used, recoil heating could be suppressed as well. Enhanced laser intensities without optical lattices and the pertinent heating effects could be achieved with optical ring resonators. Apart from their application in hybrid traps, optical lattices for ions, or ions and atoms, are themselves promising systems, for example to combine Coulomb or charge-exchange interactions with scalability for quantum simulation experiments as discussed in Refs. [7,14,16]. To avoid temporal overlap between rf and optical lattice during loading from a rf trap, turning off the rf drive faster would be advantageous. However, the ring-down time of the rf resonance circuit has to be considered as well as additional heating effects in case of nonadiabatic changes of the potentials. The limitations of our experiment in terms of lifetimes in the optical ion traps can be overcome by using high-power, far-off-resonance lasers, although the need for high powers may be reduced by employing optical cavities.

Note added.—We note that closely related results are reported in Ref. [36].

*tobias.schaetz@physik.uni-freiburg.de
[1] D. J. Wineland and D. Leibfried, Laser Phys. Lett. **8**, 175 (2011).
[2] P. Schindler, J. T. Barreiro, T. Monz, V. Nebendahl, D. Nigg, M. Chwalla, M. Hennrich, and R. Blatt, Science **332**, 1059 (2011).

[3] C. W. Chou, D. B. Hume, J. C. J. Koelemeij, D. J. Wineland, and T. Rosenband, Phys. Rev. Lett. **104**, 070802 (2010).

[4] R. P. Feynman, Int. J. Theor. Phys. **21**, 467 (1982).

[5] D. Porras and J. I. Cirac, Phys. Rev. Lett. **92**, 207901 (2004).

[6] A. Friedenauer, H. Schmitz, J. T. Glueckert, D. Porras, and T. Schaetz, Nat. Phys. **4**, 757 (2008).

[7] C. Schneider, D. Porras, and T. Schaetz, Rep. Prog. Phys. **75**, 024401 (2012).

[8] R. Islam, E. E. Edwards, K. Kim, S. Korenblit, C. Noh, H. Carmichael, G.-D. Lin, L.-M. Duan, C.-C. J. Wang, J. K. Freericks, and C. Monroe, Nat. Commun. **2**, 377 (2011).

[9] T. Monz, P. Schindler, J. T. Barreiro, M. Chwalla, D. Nigg, W. A. Coish, M. Harlander, W. Hänsel, M. Hennrich, and R. Blatt, Phys. Rev. Lett. **106**, 130506 (2011).

[10] S. Seidelin, J. Chiaverini, R. Reichle, J. J. Bollinger, D. Leibfried, J. Britton, J. H. Wesenberg, R. B. Blakestad, R. J. Epstein, D. B. Hume, W. M. Itano, J. D. Jost, C. Langer, R. Ozeri, N. Shiga, and D. J. Wineland, Phys. Rev. Lett. **96**, 253003 (2006).

[11] M. Kumph, M. Brownnutt, and R. Blatt, New J. Phys. **13**, 073043 (2011).

[12] R. J. Clark, T. Lin, K. R. Brown, and I. L. Chuang, J. Appl. Phys. **105**, 013114 (2009).

[13] J. W. Britton, B. C. Sawyer, A. C. Keith, C.-C. J. Wang, J. K. Freericks, H. Uys, M. J. Biercuk, and J. J. Bollinger, Nature (London) **484**, 489 (2012).

[14] C. Schneider, M. Enderlein, T. Huber, and T. Schaetz, Nat. Photonics **4**, 772 (2010).

[15] C. Schneider, M. Enderlein, T. Huber, S. Dürr, and T. Schaetz, Phys. Rev. A **85**, 013422 (2012).

[16] J. I. Cirac and P. Zoller, Nature (London) **404**, 579 (2000).

[17] M. Greiner and S. Fölling, Nature (London) **453**, 736 (2008).

[18] M. Cetina, A. T. Grier, and V. Vuletić, arXiv:1205.2806v2.

[19] A. T. Grier, M. Cetina, F. Oručević, and V. Vuletić, Phys. Rev. Lett. **102**, 223201 (2009).

[20] C. Zipkes, S. Palzer, C. Sias, and M. Köhl, Nature (London) **464**, 388 (2010).

[21] S. Schmid, A. Härter, and J. H. Denschlag, Phys. Rev. Lett. **105**, 133202 (2010).

[22] W. G. Rellergert, S. T. Sullivan, S. Kotochigova, A. Petrov, K. Chen, S. J. Schowalter, and E. R. Hudson, Phys. Rev. Lett. **107**, 243201 (2011).

[23] C. Cormick, T. Schaetz, and G. Morigi, New J. Phys. **13**, 043019 (2011).

[24] S. Kuhr, W. Alt, D. Schrader, M. Müller, V. Gomer, and D. Meschede, Science **293**, 278 (2001).

[25] H. Katori, S. Schlipf, and H. Walther, Phys. Rev. Lett. **79**, 2221 (1997).

[26] J. I. Cirac, R. Blatt, and P. Zoller, Phys. Rev. A **49**, R3174 (1994).

[27] R. Schmied, T. Roscilde, V. Murg, D. Porras, and J. I. Cirac, New J. Phys. **10**, 045017 (2008).

[28] T. Pruttivarasin, M. Ramm, I. Talukdar, A. Kreuter, and H. Häffner, New J. Phys. **13**, 075012 (2011).

[29] T. Schaetz, A. Friedenauer, H. Schmitz, L. Petersen, and S. Kahra, J. Mod. Opt. **54**, 2317 (2007).

[30] A. Friedenauer, F. Markert, H. Schmitz, L. Petersen, S. Kahra, M. Herrmann, T. Udem, T. W. Hänsch, and T. Schaetz, Appl. Phys. B **84**, 371 (2006).

[31] The initial temperature of $T_0 = 3.5$ mK has also been confirmed by a direct temperature measurement with a release and recapture technique [32]. Further MCS parameters are the optimized parameters of the rf trap potential from Ref. [15], $\alpha = 35°$, $\omega_{y'}^2 = -(2\pi \times 50 \text{ kHz})^2$, and $\omega_{x'} - \omega_{y'} = 2\pi \times 2.50$ kHz.

[32] C. Tuchendler, A. M. Lance, A. Browaeys, Y. R. P. Sortais, and P. Grangier, Phys. Rev. A **78**, 033425 (2008).

[33] J. P. Gordon and A. Ashkin, Phys. Rev. A **21**, 1606 (1980).

[34] A detailed analysis of the remaining dc potential [15] shows that it has to be defocusing in at least one direction. In addition, there are forces due to residual uncompensated stray fields, discussed below.

[35] J. Dalibard and C. Cohen-Tannoudji, J. Opt. Soc. Am. B **2**, 1707 (1985).

[36] R. B. Linnet, I. D. Leroux, M. Marciante, A. Dantan, and M. Drewsen, following Letter, Phys. Rev. Lett. **109**, (2012).